

Interface structure and magnetism of magnetic tunnel junctions with a Co_2MnSi electrode

J. Schmalhorst,* S. Kämmerer, M. Sacher, G. Reiss, and A. Hütten

Department of Physics, University of Bielefeld, Nano Device Group, P.O. Box 100131, 33501 Bielefeld, Germany

A. Scholl

Lawrence Berkeley National Laboratory, Berkeley, California 94720, USA

(Received 18 March 2004; published 30 July 2004)

Magnetic tunnel junctions with a magnetically soft Heusler-alloy electrode ($\text{Co}_2\text{MnSi}/\text{Al}+\text{oxidation}+\textit{in situ}$ annealing/ $\text{Co}_7\text{Fe}_3/\text{Mn}_{83}\text{Ir}_{17}$) and a maximal tunnel magnetoresistance effect of 86% at 10 K/10 mV are investigated with respect to their structural and magnetic properties at the lower barrier interface by electron and x-ray absorption spectroscopy. A plasma-oxidation-induced Mn/Si segregation and oxide formation at the barrier interface is found, which results in a strongly increased area-resistance product of the junctions, because of an enlarged barrier thickness. For Co_2MnSi thickness equal to 8 nm or larger, ferromagnetic order of Mn and Co spins at the interface is induced by annealing; simultaneously, atomic ordering at the interface is observed. The influence of the structural and magnetic interface properties on the temperature-dependent transport properties of the junctions is discussed.

DOI: 10.1103/PhysRevB.70.024426

PACS number(s): 75.70.-i, 72.25.-b, 85.75.-d

I. INTRODUCTION

The interest in magnetic tunnel junctions (MTJ) increased considerably in recent years, because MTJs are rated as a promising candidate for future sensor and memory devices.¹ Field-dependent resistance changes (tunneling magnetoresistance or TMR), of up to 60% at room temperature (RT)² have been reported for MTJs with polycrystalline magnetic electrodes. The theoretically predicted spin polarization of 100% in some Heusler alloys³ makes them very attractive for increasing the TMR effect. However, the implementation of these materials as magnetic electrodes into MTJs is a very challenging task.

The full Heusler alloy Co_2MnSi (CMS) is investigated here. Band structure calculations predict a gap at the Fermi energy for the minority electrons.⁴ These calculations also show that antisite disorder will destroy this effect, hence, precise control of the microstructure is required. Recently, we reported on the room-temperature preparation and the magnetic behavior of Co_2MnSi thin films.^{5,6} It was shown, that a vanadium seed layer induced a (110) textured growth at room temperature. A postannealing procedure was developed for these films to obtain the desired microstructural, magnetic and electrical bulk properties. In particular, a saturation magnetization of up to $4.7 \mu_B$ per unit cell was achieved.

In this work the temperature dependent transport properties of $\text{Co}_2\text{MnSi}/\text{AlO}_x/\text{Co}_{70}\text{Fe}_{30}$ MTJs is correlated to the structural and magnetic properties of the $\text{Co}_2\text{MnSi}/\text{AlO}_x$ barrier interface, which are investigated by x-ray absorption spectroscopy (XAS), x-ray magnetic circular dichroism (XMCD), Auger electron spectroscopy (AES), scanning electron microscopy (SEM), atomic force microscopy (AFM), depth profiling with AES, and x-ray photoemission electron microscopy (X-PEEM).

II. EXPERIMENT

The MTJs are prepared at room temperature by dc- and rf-magnetron sputtering on thermally oxidized Si(100) wa-

fers. A typical growth rate is 0.3 nm/s. Details of the preparation are found elsewhere.^{5,6} For investigating the $\text{Co}_2\text{MnSi}-\text{AlO}_x$ interface by surface sensitive XAS, XMCD, and AES four different half MTJs are grown:

(1) Stack A: $\text{V}^{42 \text{ nm}}/\text{Co}_2\text{MnSi}^{d(\text{CMS})}$ with $d(\text{CMS})=4, 8, 15, 61, \text{ and } 100 \text{ nm}/\text{Al}^{1.4 \text{ nm}}$ +plasma oxidation for 200 s + *in situ* annealing at about 450°C for 40 min.

(2) Stack B: $\text{V}^{42 \text{ nm}}/\text{Co}_2\text{MnSi}^{8 \text{ nm}, 100 \text{ nm}}/\text{Al}^{1.4 \text{ nm}}$ +plasma oxidation for 200 s.

(3) Stack C: $\text{V}^{42 \text{ nm}}/\text{Co}_2\text{MnSi}^{100 \text{ nm}}/\text{Al}^{1.4 \text{ nm}}$ +natural oxidation.

(4) Stack D: $\text{V}^{42 \text{ nm}}/\text{Co}_2\text{MnSi}^{100 \text{ nm}}/\text{Co}^6 \text{ nm}/\text{Al}^{1.4 \text{ nm}}$ +plasma oxidation for 200 s.

For investigating the transport properties of full MTJs a magnetically hard $\text{Co}_{70}\text{Fe}_{30}^{5 \text{ nm}}$ layer, exchange-biased by a subsequent antiferromagnetic $\text{Mn}_{83}\text{Ir}_{17}^{10 \text{ nm}}$ layer, is additionally deposited on a type A (100 nm) half junction. The upper electrode is deposited after the *in situ* annealing step without breaking the vacuum. Finally, the full MTJs are covered by an upper conduction layer and subsequently patterned by optical lithography and ion beam etching (quadratic junction area $S_J=10\,000\text{--}90\,000 \mu\text{m}^2$). The full MTJs are vacuum annealed for 1 h at 275°C in a magnetic field of 1 kOe to set the exchange bias of the upper Co-Fe electrode.

The X-PEEM and XAS/XMCD measurements in total electron yield (TEY) detection are performed at the PEEM-2 beamline 7.3.1.1 at the Advanced Light Source, Berkeley, USA. The spectra are obtained by recording the sample current as a function of the energy of right elliptically polarized x-rays (degree of circular polarization $P_{hv}=75\%$). For XAS normal incidence is used, for XMCD the angle of incidence for the x-rays is $\theta=30^\circ$ with respect to the surface. XMCD spectra are taken by saturating the sample in an alternating magnetic field applied along the x-ray propagation direction (the corresponding TEY spectra are denoted by I^+ and I^-). The remanent domain state of the samples is investigated by X-PEEM with $\theta=30^\circ$. For AES and depth profiling a scan-

ning Auger microscope phi 660 is used. The samples are continuously rotated during sputtering with a 500 eV Ar^+/Xe^+ ion beam (angle of incidence 70° with respect to the surface normal) to achieve optimum depth resolution. The Auger electrons are excited by a 10 keV/200 nA electron beam, which is scanned over an area of about $70 \mu\text{m}$ diameter. The measured Auger intensities $I_j(t)$ [defined as peak to peak heights of the differential spectrum $d(EN)/dE$] of the different components j are converted into atomic concentrations $X_j(t)$ by using relative sensitivity factors S_j for the individual Auger lines.^{7,8} The surfaces of selected samples are investigated by AFM (Digital Instruments Nanoscope IIIa) and SEM (LEO Gemini).

The TMR ($\equiv [R_{\text{max}} - R_{\text{min}}]/R_{\text{min}}$) is measured as a function of temperature ranging from 10 K up to RT. The external magnetic field H for measuring the magnetoresistance is applied (anti-)parallel to the exchange-bias direction of the Co-Fe electrode.

III. EXPERIMENTAL RESULTS

A. Tunnel magnetoresistance and area resistance product

At first, the full magnetic tunnel junctions with a 100 nm thick type A Co_2MnSi electrode (MTJ-CMS) are compared to optimized full $\text{Mn}_{83}\text{Ir}_{17}/\text{Co}_{70}\text{Fe}_{30}/\text{AlO}_x/\text{Ni}_{80}\text{Fe}_{20}$ MTJs (MTJ-NiFe) with respect to their temperature dependence of the TMR. Details of the preparation and the properties of the MTJ-NiFe having polycrystalline Ni-Fe and Co-Fe electrodes can be found elsewhere.⁹ The low temperature and low bias voltage major loop of MTJ-CMS is shown in Fig. 1(a). A maximum TMR of 86% is found. The switching of the soft Co_2MnSi and the pinned Co_7Fe_3 electrode is marked with arrows. Because of the limited external field that can be applied during measurement, the pinned electrode is not completely saturated at negative magnetic fields. Furthermore, the strong increase of the coercivity of the Co-Fe at low temperature hinders the perfect antiparallel alignment of the electrodes in zero magnetic fields, which slightly reduces the maximum resistance R_{max} and accordingly the TMR.

If the temperature dependent TMR of MTJ-CMS and MTJ-NiFe are compared, three experimental facts are of major importance which have to be explained on the basis of structural and magnetic interface properties:

(1) The minimal area resistance product $R_{\text{min}} = 13.3 \text{ G}\Omega \mu\text{m}^2$ of MTJ-CMS is about 400 times higher than that of MTJ-NiFe, although the Al thickness prior to oxidation is identical (1.4 nm) and the oxidation conditions are comparable. At room temperature MTJ-NiFe is characterized⁹ by a mean barrier height of $2.89 \pm 0.10 \text{ eV}$ and a barrier thickness of $1.76 \pm 0.09 \text{ nm}$. Therefore, an increase of the barrier thickness of only 5 \AA for MTJ-CMS can account for its higher resistance because of the exponential dependence of the area resistance product on the barrier thickness for direct tunneling.¹⁰

(2) The TMR at 10 K is significantly higher for MTJ-CMS (86% instead of 71%). If the Julliere model¹¹ is used for relating the TMR effect to the effective spin polarizations

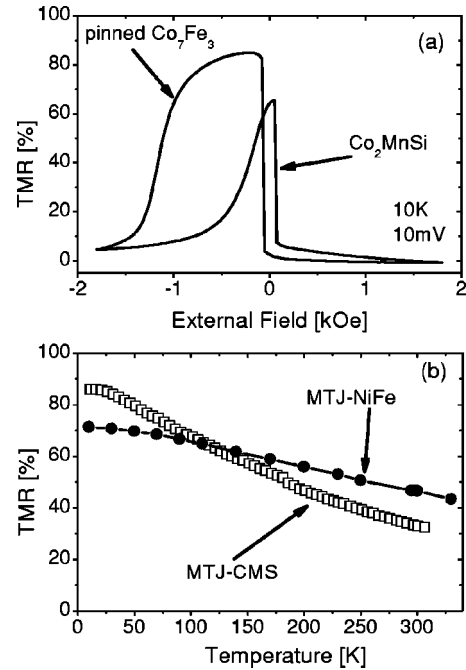


FIG. 1. (a) TMR major loop of MTJ-CMS. The measurement is performed at 10 K with 10 mV bias; (b) TMR temperature dependence of MTJ-CMS and MTJ-NiFe (Ref. 9). The measurements are performed at 10 mV bias voltage.

of the electrodes, $\text{TMR} = 2P_{\text{CMS}}P_{\text{CoFe}}/[1 - P_{\text{CMS}}P_{\text{CoFe}}]$, the TMR of 86% for MTJ-CMS corresponds to $P_{\text{CMS}} = 61\%$, because the low temperature spin polarization of Co_7Fe_3 is $P_{\text{CoFe}} = 49\%$ in our MTJs with AlO_x barrier.¹² Although the desired spin polarization of 100% is not reached yet, it has to be emphasized that the experimental value of $P_{\text{CMS}} = 61\%$ is larger than the effective spin polarization of a variety of 3d-transition metal alloys in combination with Al_2O_3 barriers limited to maximal 55%.¹³

(3) The temperature dependence of the TMR is more pronounced for MTJ-CMS.

For understanding this behavior the knowledge of the structural and magnetic interface properties is of paramount importance, because the Heusler alloys are very sensitive to atomic disorder.^{4,14}

B. Surface topography and magnetic microstructure of the Co_2MnSi electrode

The surface topography of the half MTJs is investigated by SEM. For type B samples (not annealed after sputter deposition) no topographical contrast is found for layer thickness up to $d(\text{CMS}) = 100 \text{ nm}$ but the *in situ* annealed samples (type A) have a pronounced topographical contrast resulting from individual grains, slightly tilted with respect to each other [see Fig. 2(a)]. The typical in-plane grain size G of the Co_2MnSi electrode increases strongly with increasing layer thickness from about $G = 100 \text{ nm}$ for $d(\text{CMS}) = 15 \text{ nm}$ up to $G = 300 \text{ nm}$ for $d(\text{CMS}) = 100 \text{ nm}$. The driving force for the grain growth during *in situ* annealing is the reduction of the grain boundary energy. As shown in Sec.

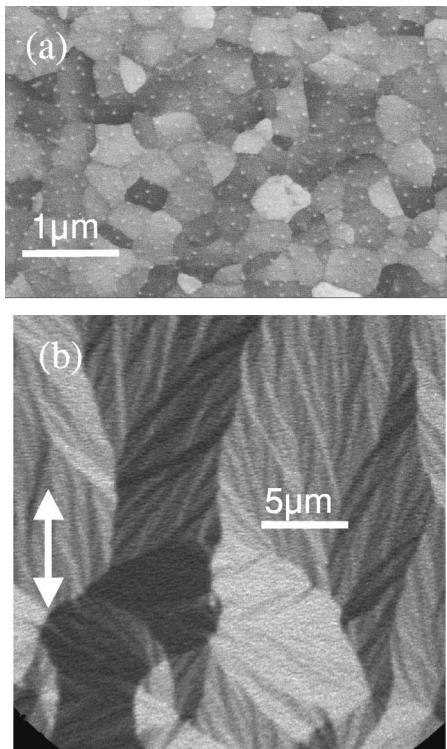


FIG. 2. (a) Typical 20 kV SEM micrograph of type A sample: $V^{42} \text{ nm}/\text{Co}_2\text{MnSi}^{100} \text{ nm}/\text{Al}^{1.4} \text{ nm} + \text{oxidation} + \text{in situ}$ annealing; (b) X-PEEM image (Mn L edge) of the not magnetized sample. The Mn L_3 image is divided by the Mn L_2 image to increase the contrast. White arrows mark the sensitivity direction.

III A, the ~ 2 nm thin tunnel barrier can successfully sustain the variation of the mechanical stress during grain growth and is not shorted.

AFM measurements are performed to determine the tilt of the individual grains with respect to the film plane. Even for the sample with the thickest Co_2MnSi layer (100 nm) and, therefore, largest grains the maximum tilt is only 0.3° . Because of the high (110)-texture and the small tilt angles of the grain surfaces with respect to the film plane, the Co_2MnSi grains are terminated with (110)-planes (possible modifications in the atomic and magnetic order of the interface will be discussed below). The surface roughness of the barrier is not significantly altered by the *in situ* annealing process., e.g., for $d(\text{CMS})=100$ nm the rms roughness of stack A and stack B is 0.41 and 0.44 nm, respectively. The X-PEEM image of the type A sample with $d(\text{CMS})=100$ nm at the Mn $L_{2,3}$ edges [Fig. 2(b)] clearly shows its magnetically soft behavior. The original domain state, i.e., the sample is *not* saturated after preparation, is characterized by several μm large domains superimposed on a magnetization ripple due to local fluctuations of the crystalline anisotropy and flux closure.

C. Atomic concentration study of the $\text{Co}_2\text{MnSi}-\text{AlO}_x$ interface

As discussed in our previous work,⁵ the Co_2MnSi alloy only orders atomically and magnetically during the *in situ* annealing process. Therefore, in principle, a thermally in-

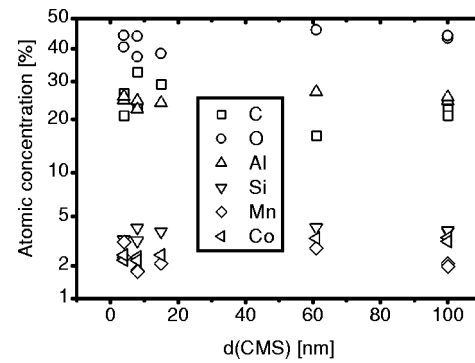


FIG. 3. Atomic concentration of type A samples as a function of Co_2MnSi thickness.

duced segregation of some alloy components at the barrier interface or a diffusion of vanadium from the seed layer to the barrier is possible. This is addressed by AES investigations of the surfaces of the half MTJ stacks A–C.

The AES results are summarized in Fig. 3. For all type A samples with Co_2MnSi thickness ranging from $d(\text{CMS})=4$ to 100 nm no vanadium is detected, a vanadium diffusion during the *in situ* annealing from the 42 nm thick buffer to the lower barrier interface can be ruled out. All samples show a C contamination of typically 20%–30% at the surface, which results from the sample transport and storage in air (the localization of the C only at the surface of the samples is proved by depth profiling). Please note, that the depth profile of the full MTJ-CMS, gives no hint to a C contamination at the upper barrier interface (the full junctions are deposited without vacuum break).

The measured atomic concentrations X_i of O, Al, Co, Mn, and Si show no clear trend within the scatter of the data for different Co_2MnSi thicknesses. The atomic concentration X_i of Si, Mn, and Co is strongly reduced by the covering AlO_x layer. The reduction of the Mn2 (586 eV), the Co1 (772 eV) and the Si2 (1615 eV) signal by a thin Al_2O_3 layer calculated with *NIST Electron Effective-Attenuation-Length Database*^{15,16} can be well described by a first-order exponential decay with effective decay lengths of $\lambda_{\text{Mn}_2}^{\text{eff}}=1.01$ nm, $\lambda_{\text{Co}_1}^{\text{eff}}=1.28$ nm, and $\lambda_{\text{Si}_2}^{\text{eff}}=2.41$ nm, respectively. The resulting intensity reduction of these three Auger peaks leads to measured atomic concentrations differing significantly from the true atomic concentrations at the $\text{Co}_2\text{MnSi}-\text{AlO}_x$ interface. The measured X_{Si} is considerably enhanced with respect to X_{Co} and X_{Mn} , X_{Co} with respect to X_{Mn} . After correcting this effect in the first order¹⁷ and averaging the resulting relative concentrations of Si, Mn, and Co with respect to the Heusler film thickness, a corrected composition of $\bar{X}_{\text{type A}} = \text{Co}_{34\pm 1}\text{Mn}_{41\pm 2}\text{Si}_{24\pm 1}$ below the AlO_x is found.

For checking the influence of the *in situ* annealing on the atomic concentrations of stack A, these samples are compared with the not annealed type B samples. After correcting the influence of the EAL effect¹⁷ and averaging with respect to the layer thickness, the corrected composition of the type B samples is $\bar{X}_{\text{type B}} = \text{Co}_{36\pm 4}\text{Mn}_{43\pm 6}\text{Si}_{21\pm 2}$ in accordance with $\bar{X}_{\text{type A}}$. Therefore, the in-situ annealing procedure does not significantly alter the measured atomic concentrations, and,

accordingly, thermally induced segregation processes at the $\text{Co}_2\text{MnSi}-\text{AlO}_x$ interface are not very pronounced.

The atomic concentration at the interface may also be altered during the plasma oxidation process. To check this, the deviation of the corrected composition of type A and B samples from the ideal bulk composition of $\text{Co}_{50}\text{Mn}_{25}\text{Si}_{25}$ must be analyzed. The relative sensitivity factors used for quantification of the Auger intensities⁷ base on reference measurements of elemental samples, i.e., pure Si, Mn, and Co. This may result in systematic errors due to matrix effects.⁷ To overcome this problem the type C sample is used as a reference. It is not annealed, ruling out thermally induced surface segregation of some components. Furthermore, the naturally oxidized 1.4 nm thick Al layer protects the buried Heusler surface from oxygen, because the natural oxidation depth is limited to about 1 nm. The electron attenuation effect is corrected in the same way as for the type A and B samples. Although the natural oxidation of the 1.4 nm thick Al layer leads to an AlO_x/Al capping bilayer, the electron attenuation can be simulated by a single 1.8 nm thick Al_2O_3 layer, since the calculated¹⁵ attenuation by an Al layer is very similar to the attenuation by the same layer when it is completely oxidized. The corrected reference concentration for the type C sample is $X_{\text{type C}} = \text{Co}_{47}\text{Mn}_{36}\text{Si}_{17}$. The comparison with the data of the plasma oxidized samples $\bar{X}_{\text{type B}} = \text{Co}_{36\pm 4}\text{Mn}_{43\pm 6}\text{Si}_{21\pm 2}$ and $\bar{X}_{\text{type A}} = \text{Co}_{34\pm 1}\text{Mn}_{41\pm 2}\text{Si}_{24\pm 1}$ reveals a Mn and Si segregation during plasma oxidation.

The probable driving force for the segregation is the formation of MnO_x (this will be verified in Sec. III D) and SiO_x at the lower barrier interface because of their large oxygen affinity.¹⁸ For roughly estimating the barrier thickness of plasma oxidized samples, depth profiling of a type A sample (100 nm thick Co_2MnSi) and the type D sample is performed. The thickness of the insulating barrier is estimated from the sputtering time needed to remove the oxidized surface layer (assumed to be proportional to the thickness). For the type A sample, this sputtering time is about 1/3 larger than for the type D sample. Accordingly, the insulating barrier for the type A sample is about $1/3 \times 1.8 \text{ nm} = 0.6 \text{ nm}$ thicker. The increased barrier thickness explains the high area resistance product of MTJ-CMS discussed in Sec. III A.

D. Magnetic interface properties and chemical states of half MTJs

The half MTJ stacks A, B, and C are now discussed with respect to their element specific magnetic and chemical properties measured by XAS and XMCD. Typical XAS measurements (normal incidence) of Co and Mn are shown in Fig. 4. As already mentioned in Sec. III C, the natively oxidized Al cap layer prevents the oxidation of the buried Co_2MnSi surface below the oxidized Al film for the type C sample. The XAS spectrum of Co is characterized by structureless $L_{2,3}$ absorption edges, which are typical for Co with delocalized $3d$ electrons (e.g., metallic Co) but the resonance lines for the Co_2MnSi films are significantly wider than for pure Co.¹⁹ This hints at strong changes of the bandstructure at the Co sites in the Heusler alloy with respect to the pure metallic Co.

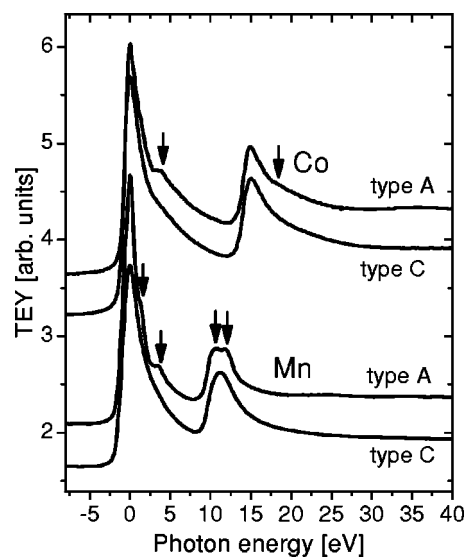


FIG. 4. XAS spectra of a type A and a type C sample with $d(\text{CMS})=100 \text{ nm}$. The photon energy is defined with respect to the maximum of the L_3 absorption edge. The arrows indicate additional features in the XAS of type A samples in comparison to the type C sample.

The XAS spectrum at the Co $L_{2,3}$ edge for the type A sample (100 nm Co_2MnSi , see Fig. 4) shows an additional shoulder at $\sim 4 \text{ eV}$ above the maxima of the $L_{2,3}$ intensities but the observed absorption edge shape is neither compatible with pure metallic Co nor with the typical multiplet structure of CoO .¹⁹ Although the type A sample (as well as all other type A samples and the type B sample) is plasma oxidized for 200 s resulting in the Mn/Si segregation, we have no indication for the presence of CoO in the near barrier region.

All type A samples with Co_2MnSi thickness ranging from 8 to 100 nm show the additional 4 eV feature, only the type A sample with the thinnest Co_2MnSi layer (4 nm) and the type B sample do not. As will be discussed, this perfectly accords with a significant (or, respectively, for the latter samples a vanishing) XMCD signal indicating ordered interfacial spins. Therefore, this additional feature can be attributed to certain atomic and magnetic orders of the Co_2MnSi alloy at the lower barrier interface.

For Mn, the situation is different (see Fig. 4). The type C sample shows a structureless $L_{2,3}$ absorption edge shape typically for delocalized $3d$ electrons, like in metallic Mn.²⁰ In contrast, all plasma oxidized samples (type A and type B) have a pronounced multiplet structure (indicated by the arrows in the lower part of Fig. 4), independent from Co_2MnSi thickness and annealing procedure. The multiplet structure clearly hints at an increased localization of the $3d$ electrons. The energy positions of the additional peaks agree quite well with calculated XAS spectra assuming a ${}^6S_{5/2}$ ground-state term.²¹ Especially, this line shape is found for oxidized Mn.²⁰ As shown in Sec. III C a Mn/Si segregation at the lower barrier interface for plasma oxidized samples is observed. The formation of MnO_x is now verified by the development of the Mn-multiplet structure in all plasma oxidized samples (up to now, the chemical state of Si in the segregation layer

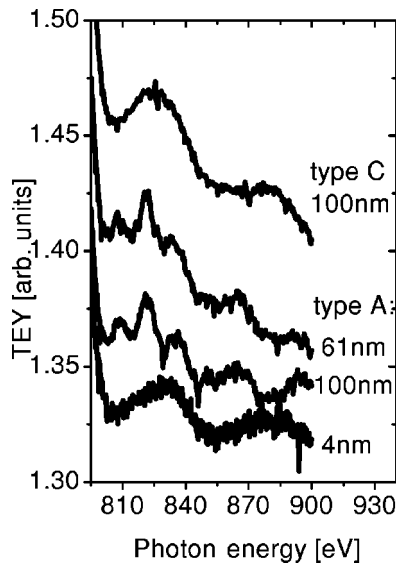


FIG. 5. Post edge region of the Co $L_{2,3}$ edges for some type A samples (4, 61, and 100 nm Co_2MnSi thickness) and the type C sample.

could not be investigated by XAS because of experimental restrictions). Usually, the MnO_x multiplet structure for pure oxide films is significantly sharper.²² This means, that the measured shape of the Mn $L_{2,3}$ edges of all plasma oxidized type A and B samples results from a superposition of a signal from MnO_x in the segregation layer and a signal from the underlying (not oxidized) Mn of the Heusler alloy. In contrast to Co, which showed the additional shoulder 4 eV above the resonances, no clearly visible change of the absorption edge shape after annealing is found.

In Heusler alloys the bulk magnetic and atomic order are correlated,^{4,5,14} the same is expected to hold at the interface. The atomic interface order of the Heusler alloy can be studied by analyzing the XAS spectra of Co with respect to their extended x-ray absorption fine structure (EXAFS).²³ Due to the surface sensitivity of XAS in TEY detection EXAFS contains information about the local environment of Co atoms at the interface. The post edge region of the Co $L_{2,3}$ edges (see Fig. 5) shows the same EXAFS oscillations for all types of A samples with $d(\text{CMS})$ ranging from 8 to 100 nm. For all

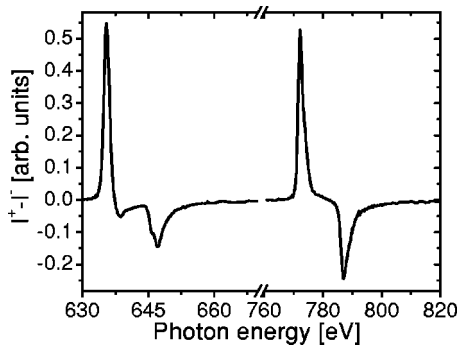


FIG. 6. Typical XMCD asymmetry $I^+ - I^-$ of Mn and Co (type A sample, Co_2MnSi thickness 100 nm).

other samples the EXAFS oscillations have a much larger period as a function of photon energy. This indicates, that the atomic interface order of those samples is significantly different than for the type A samples with $d(\text{CMS}) \geq 8$ nm.

The relative XMCD signal A_{total} is defined as

$$A_{\text{total}} = -\frac{-6p + (8/3)q}{rP_{h\nu} \cos \theta}$$

with

$$r = \int_{L_3+L_2} (I^+ + I^- - s.f.) dE$$

$$p = \int_{L_3} (I^+ - I^-) dE$$

$$q = \int_{L_3+L_2} (I^+ - I^-) dE,$$

and with I^+ and I^- the TEY signal of the sample saturated in a positive ($\vec{M} \downarrow \uparrow \vec{P}$) and a negative ($\vec{M} \uparrow \uparrow \vec{P}$) magnetic field. The data taken at 30% grazing incidence are normalized with respect to the current in the storage ring and the transmission function of the monochromator. The background function $s.f.$ is a two-step-function with thresholds set to the peak positions of the L_3 and L_2 white lines and with relative step heights of $2/3$ (L_3) and $1/3$ (L_2). This definition of A_{total} will be used to compare the different samples qualitatively with respect to their element specific magnetic interface properties. Please note, that according to the XMCD sum rules²⁴ this definition of A_{total} is equivalent to the total magnetic moment given in units of μ_B per atom and number of $3d$ holes (spin magnetic dipole term $\langle T_z \rangle$ neglected), if the XMCD sum rules²⁴ were applicable without any restriction. The number of $3d$ holes can be taken from band structure calculations, but a fully quantitative interpretation is complicated by several factors: For Mn the $2p-3d$ electrostatic interaction becomes important.^{20,25} This leads to jj mixing, which is neglected in the XMCD sum rules. Nakajima *et al.*²⁶ showed, that the electron yield saturation effect can reduce the measured magnetic spin moment m_s by 10%–20%, the influence on the orbital moment m_l is even worse. Further complications result from spin- and energy-dependent variation of the TEY²⁷ and the neglect of the spin dipole term $\langle T_z \rangle$.²⁸

Typical measurements of the XMCD asymmetry $I^+ - I^-$ for Mn and Co are shown in Fig. 6. The relative XMCD signals A_{total} for all type A and B samples are summarized in Fig. 7. The XMCD asymmetry has the same sign for Mn and Co, the element specific magnetic interface moments are aligned parallel to each other. The shape of the asymmetry is independent of the Co_2MnSi layer thickness from 8 to 100 nm for all type A samples. Therefore, the ratio of the orbital and the spin magnetic moment (m_l/m_s) of those samples does not depend on the Co_2MnSi thickness. Only for the type A

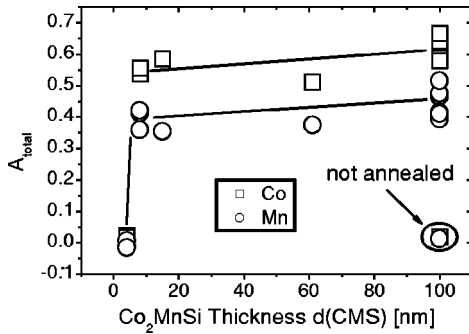


FIG. 7. Summary of the relative XMCD signal A_{total} of Mn and Co for stack A and B samples. The results of the type B sample are labeled with *not annealed*. The lines are guides to the eye.

sample with $d(\text{CMS})=4$ nm and the type B sample no XMCD signal is detected and, hence, the interfacial magnetic moments are not ferromagnetically ordered. This is closely related to the magnetic bulk properties investigated by magnetometry. Only for $d(\text{CMS}) \geq 8$ nm and after *in situ* annealing a magnetic bulk moment of $4.3\text{--}4.4 \mu_B$ close to the expected value of $5 \mu_B$ ¹⁴ is found.

Furthermore, the interfacial magnetic order is correlated to the certain atomic order indicated by the Co EXAFS oscillations found for type A samples with $d(\text{CMS}) \geq 8$ nm. Indeed, the correlation of atomic and magnetic order is a typical fingerprint for full Heusler alloys.^{4,14}

The A_{total} of type A samples increases rapidly by increasing the film thickness from 4 to 8 nm. For larger $d(\text{CMS})$ a further slight increase of A_{total} is found for Mn (Co) from 0.40 ± 0.02 (0.55 ± 0.01) at $d(\text{CMS}) = 8$ nm to 0.44 ± 0.02 (0.60 ± 0.01) for $d(\text{CMS}) = 100$ nm. This is accompanied by the increase of the grain sizes (see Sec. III B). Band structure calculations²⁹ give the numbers of $3d$ holes for Co (2.24) and Mn (4.52). To correct the jj mixing for Mn its spin moment m_s is multiplied by the factor χ .²⁰ The value of χ is not precisely known, but lies in the range from 1.0 (Ref. 30) to 1.5.²⁰ Neglecting all other complications of the applicability of the sum rules mentioned above, the ratio of the total magnetic moments for Co and Mn can be estimated in first order. For $d(\text{CMS}) = 100$ nm this gives $m^{\text{Mn}}/m^{\text{Co}} = 1.5\text{--}2.2$ (depending on the values for χ), from bandstructure calculations a magnetic moment ratio of $m^{\text{Mn}}/m^{\text{Co}} \approx m_s^{\text{Mn}}/m_s^{\text{Co}} = 2.9$ ³¹ is expected (the calculated orbital moments for Co and Mn³² as well as the total magnetic moment of Si^{31,32} are very small and can be neglected here). A reduced magnetic moment ratio is reasonable, because of (1) the MnO_x formation in the segregation layer (Mn oxides are usually paramagnetic at RT) and (2) the residual atomic disorder in the interface region because of the segregation. The low temperature magnetic properties of the Mn ions in the segregation layer as well as the temperature dependence of A_{total} for Mn and Co will be addressed by temperature dependent XMCD investigations in the near future.

The reasons for the vanishing bulk/interface magnetic order for $d(\text{CMS})=4$ nm at room temperature are not clear up to now. It may result from structural differences in the as-grown films between the nucleation zone (i.e., adjacent to the

V seed layer) and the surface of the film. Depth profiles of type A and B samples with $d(\text{CMS})=8$ nm showed, that a weak interdiffusion at the V/ Co_2MnSi interface during *in situ* annealing at 450°C is present. Both may result in higher atomic disorder in the nucleation zone quenching the magnetic moments at room temperature.

E. Discussion

Finally, the structural and magnetic properties of the $\text{Co}_2\text{MnSi}/\text{AlO}_x$ interface have to be discussed with respect to the transport properties of the full MTJ-CMS.

The high area resistance product results from the larger barrier thickness because of Mn/Si segregation and oxide formation. The first reason for the limitation of the tunneling spin polarization to 61% up to now is atomic disorder^{4,14} at the interface. The plasma oxidation induced segregation results in an inhomogeneous distribution of the atoms in the interface region as a function of depth, making perfect atomic order of the Co_2MnSi impossible. For elevated temperatures the disorder results in enhanced magnon scattering³³ of the tunneling electrons, which deteriorates the TMR temperature dependence. Second, the presence of paramagnetic ions in the barrier may reduce the TMR effect.³⁴ The oxidation induced segregation results in Mn ions that are located in the extended tunneling barrier. Mn ions usually are paramagnetic and, therefore, can act as scattering centers for tunneling electrons. Furthermore, the stronger temperature dependence of the TMR for MTJ-CMS in comparison with MTJ-NiFe indicates, that the density of unpolarized defect states in the tunneling barrier^{9,35} is higher for MTJ-CMS. This is reasonable because of the mechanical stress during the thermally induced grain growth in MTJ-CMS.

IV. CONCLUSIONS

In summary, magnetic tunnel junctions with a magnetically soft Heusler alloy electrode ($\text{Co}_2\text{MnSi}/\text{Al}+\text{oxidation} + \textit{in situ}$ annealing/ $\text{Co}_7\text{Fe}_3/\text{Mn}_{83}\text{Ir}_{17}$) and a maximal tunnel magnetoresistance effect of 86% at 10 K/10 mV are investigated with respect to their structural and magnetic properties at the lower barrier interface for different Co_2MnSi thickness, oxidation methods, and annealing procedures. A plasma oxidation induced Mn/Si segregation at the lower barrier interface is found, which depends neither significantly on the Co_2MnSi thickness, nor on the subsequent *in situ* annealing at 450°C . The segregation results in a strong increase of the area resistance product of MTJ-CMS in comparison to optimized Co-Fe/ AlO_x /Ni-Fe junctions with equal Al layer thickness prior to oxidation. As for bulk Co_2MnSi , *in situ* annealing induces ferromagnetic order of Mn and Co magnetic moments at the interface for Co_2MnSi thickness ≥ 8 nm; simultaneously, a certain atomic ordering at the interface is indicated by the Co EXAFS oscillations. The magnetic moments of Mn and Co are aligned parallel. An estimation of the ratio of the total magnetic moments for Mn and Co showed, that $m^{\text{Mn}}/m^{\text{Co}}$ is smaller than expected from band structure calculations because of the formation of paramagnetic Mn ions in the segregation layer and residual

disorder at the interface. The spin scattering of tunneling electrons on these ions, the residual interfacial atomic disorder due to the segregation, enhanced magnon scattering as well as a higher contribution of unpolarized defect states on the conductance are the main reasons for the current limitation of the effective spin polarization to 61% instead of 100% predicted by theory and a higher temperature dependence of the TMR in comparison to optimized Co-Fe/AIO_x/Ni-Fe junctions.

ACKNOWLEDGMENTS

The authors gratefully acknowledge the opportunity to use the beamline 7.3.1.1 at the Advanced Light Source, Berkeley (USA) and H. Brückl and A. Thomas for discussion. Two of the authors (J.S. and A.H.) gratefully acknowledge the Deutsche Forschungs Gesellschaft for financial support. The work is also supported by the U. S. Department of Energy under Contract No. DE-AC03-76SF00098.

*Electronic address: jschmalh@physik.uni-bielefeld.de

- ¹J. Daughton, J. Appl. Phys. **81**, 3758 (1997).
- ²M. Tsunoda, K. Nishikawa, S. Ogata, and M. Takahashi, Appl. Phys. Lett. **80**, 3135 (2002).
- ³R. K. de Groot, F. M. Mueller, P. G. van Engen, and K. H. J. Buschow, Phys. Rev. Lett. **50**, 2024 (1983).
- ⁴S. Ishida, T. Masaki, S. Fujii, and S. Asano, Physica B **245**, 1 (1998).
- ⁵S. Kämmerer, S. Heitmann, D. Meyners, D. Sudfeld, A. Thomas, A. Hütten, and G. Reiss, J. Appl. Phys. **93**, 7945 (2003).
- ⁶S. Kämmerer, A. Thomas, A. Hütten, and G. Reiss, Appl. Phys. Lett. **85**, 79 (2004).
- ⁷D. Briggs and M. P. Seah, *Practical Surface Analysis* (Wiley, New York, 1990), Chap. 5.
- ⁸The relative sensitivity factors S_j used throughout in this paper are taken from the *Physical Electronics MultiPak V5.0a* software: C1(Auger line)/0.076(S_j), O1/0.212, Al2/0.105, Mn2/0.161, Co1/0.226 and Si2/0.071.
- ⁹J. Schmalhorst and G. Reiss, Phys. Rev. B **68**, 224437 (2003).
- ¹⁰W. F. Brinkman, R. C. Dynes, and J. M. Rowell, J. Appl. Phys. **41**, 1915 (1970).
- ¹¹M. Julliere, Phys. Lett. **54A**, 225 (1975).
- ¹²A. Thomas, Ph.D. thesis, University of Bielefeld, Germany, 2004.
- ¹³P. LeClair, Ph.D. thesis, Eindhoven University of Technology, Netherlands, 2002.
- ¹⁴S. Picozzi, A. Continenza, and A. J. Freeman, Phys. Rev. B **69**, 094423 (2004).
- ¹⁵C. J. Powell and A. Jablonski, *NIST Electron Effective-Absorption-Length Database, Version 1.0* (National Institute of Standards and Technology, Gaithersburg, MD, 2001).
- ¹⁶The assumed material parameters for Al_{0.4}O_{0.6} are: density $\rho = 3.98$ g/cm³, number of valence electrons per molecule $N_V = 4.8$, band gap energy $E_G = 8$ eV, emission angle $\phi = 42^\circ$.
- ¹⁷The correction is done by calculating the fraction of electrons F_i with kinetic energies corresponding to the Si2, Co1, and Mn2 lines passing a 1.8 nm thick Al₂O₃ cap layer without energy loss, i.e., no inelastic scattering occurs: $F_i = \exp(-1.8 \text{ nm}/\lambda_i^{\text{eff}})$. Then, the measured concentrations X_i are divided by F_i . Finally, these values are normalized to obtain the relative concentration of Co, Mn, and Si at the interface. We assumed an Al₂O₃ thickness of 1.8 nm as a result of an optimum oxidization of only the 1.4 nm thick metallic Al layer (Ref. 36).
- ¹⁸J. A. Dean, *Langes Handbook of Chemistry, Table 9-1* (McGraw-Hill, New York, 1973).
- ¹⁹T. J. Regan, H. Ohldag, C. Stamm, F. Nolting, J. Lüning, J. Stöhr, and R. L. White, Phys. Rev. B **64**, 214422 (2001).
- ²⁰Y. Yonamoto, T. Yokoyama, K. Amemiya, D. Matsumura, and T. Ohta, Phys. Rev. B **63**, 214406 (2001).
- ²¹B. T. Thole, R. D. Cowan, G. A. Sawatzky, J. Fink, and J. C. Fuggle, Phys. Rev. B **31**, 6856 (1985).
- ²²The less sharp MnO_x multiplet for the samples discussed in this work is not a result of a limited energy resolution in XAS.
- ²³*X-Ray Absorption: Principles, Applications, Techniques of EXAFS, SEXAFS and XANES*, in Chemical Analysis 92, edited by D. C. Koningsberger and R. Prins (Wiley, New York, 1988).
- ²⁴C. T. Chen, Y. U. Idzerda, H.-J. Lin, N. V. Smith, G. Meigs, E. Chaban, G. H. Ho, E. Pellegrin, and F. Sette, Phys. Rev. Lett. **75**, 152 (1995).
- ²⁵H. A. Dürr, G. van der Laan, D. Spanke, F. U. Hillebrecht, and N. B. Brookes, Phys. Rev. B **56**, 8156 (1997).
- ²⁶R. Nakajima, J. Stöhr, and Y. U. Idzerda, Phys. Rev. B **59**, 6421 (1999).
- ²⁷V. Chakarian, Y. U. Idzerda, and C. T. Chen, Phys. Rev. B **57**, 5312 (1998).
- ²⁸R. Wu and A. J. Freeman, Phys. Rev. Lett. **73**, 1994 (1994).
- ²⁹I. Galanakis (private communication): the given numbers of 3d holes based on the work of Galanakis *et al.* (Ref. 31).
- ³⁰E. Göring (private communication).
- ³¹I. Galanakis, P. H. Dederichs, and N. Papanikolaou, Phys. Rev. B **66**, 174429 (2002).
- ³²I. Galanakis (private communication): the orbital moments calculated by using the fully relativistic code described by Mavropoulos *et al.* (Ref. 37) are 0.029 μ_B for Co, 0.017 μ_B for Mn and 0.001 for Si.
- ³³A. M. Bratkovsky, Appl. Phys. Lett. **72**, 2334 (1998).
- ³⁴R. Jansen and J. S. Moodera, Phys. Rev. B **61**, 9047 (2000).
- ³⁵C. H. Shang, J. Nowak, R. Jansen, and J. S. Moodera, Phys. Rev. B **58**, R2917 (1998).
- ³⁶R. Jansen and J. S. Moodera, Appl. Phys. Lett. **75**, 400 (1999).
- ³⁷P. Mavropoulos, K. Sato, R. Zeller, P. H. Dederichs, V. Popescu, and H. Ebert, Phys. Rev. B **69**, 054424 (2004).